RSC Applied Polymers

ROYAL SOCIETY OF CHEMISTRY

PAPER

View Article Online
View Journal

Cite this: DOI: 10.1039/d6lp00009f

Multi-dynamic bond reinforced polyurethane elastomer with outstanding damping characteristics and mechanical properties

Shaolong Li,[a] Feng Qi,*[a,b] Chunyang Di,[b] Yongpeng Yang,[a] Yang Zhao,[a] Yutong Li,[a] Hongjia Song,[a] Jinbin Wang,[a] Zhao Fu *[a] and Xiangli Zhong *[a]

Polyurethane elastomer (PUE) has become an ideal material for vibration damping and noise reduction due to its outstanding viscoelastic and molecular structural designability. However, existing materials generally struggle to overcome the effects of temperature changes because of their narrow glass transition range. Here, we innovatively synthesized a novel chain extender (HDF) using 5-hydroxymethylfurfural and 2,2′-diaminodiphenyl disulfide as raw materials, and introduced it together with isophorone diisocyanate into the PUE. The PUE cured with HDF exhibits outstanding damping properties, which are mainly attributed to the reversible exchange of dynamic bonds within its molecular network and the disruption of segment regularity caused by the irregular alicyclic structure of Isophorone diisocyanate. Experimental results demonstrate that PUE-HDF exhibits a broad effective damping temperature range of –19 to 115 °C and a high tan δ of 1.38. Additionally, the tan δ remains above 0.6 over the vibration temperature range of –15 °C to 40 °C. Notably, the tensile strength and elongation at break of the PUE increased to 19.1 MPa and 626%, respectively. This study develops a high-performance PUE damping material, aiming to further advance the development and application of dynamic bonds for reducing vibration and noise.

Received 14th January 2026,
Accepted 23rd April 2026

DOI: 10.1039/d6lp00009f

rsc.li/rscapplpolym

1. Introduction

The widespread application of mechanical equipment such as stamping machinery, centrifugal pumps, and household appliances has boosted production efficiency while simultaneously causing increasingly severe vibration and noise issues. These problems may lead to reduced equipment precision and pose potential risks to the surrounding environment and human health. In this background, developing highly efficient vibration reduction and noise suppression technologies has become particularly significant.[1,2] Damping materials serve as the key medium for converting vibrational energy, playing an indispensable role in suppressing vibrations and extending equipment service life by transforming mechanical energy into heat. Polyurethane elastomer (PUE) has been investigated due to its high viscoelastic properties and high internal friction.[3,4] However, the effective damping temperature range (EDTR) of classical PUE is usually short (20–50 °C), and its damping performance suffers considerably above room temperature. This severely limits its practical application in common high-temperature scenarios such as industrial production workshops, tropical outdoor facilities, and automotive engine compartments.[5,6] Thus, how to significantly expand the EDTR of PUE while maintaining high damping performance has become a key challenge in enhancing its practical application.

To broaden the applicability of materials over a wide temperature range, it has been demonstrated that rational molecular design and optimization of the microstructure of elastomer components are essential strategies for improving energy dissipation properties.[7] Currently, the main design approaches include constructing gradient structures,[8–10] introducing suspension chains,[11–13] establishing interpenetrating polymer networks,[14–16] adding nanofillers,[17–19] and incorporating dynamic bonds,[20–22] *etc*. Dynamic disulfide bonds have received extensive attention from researchers in recent years because of their excellent reversible exchange properties. Current research on dynamic disulfide bonds primarily focuses on synergistic interactions with catalysts or pendants to enhance material damping properties.[23,24] However, while pursuing high damping performance, this strategy also brings the problems of mechanical property degradation and increased complexity of preparation processes. For instance, Xiao *et al.*[25] enhanced the damping temperature range and heat resistance of polyurethane elastomers by introducing dynamic disulfide bonds and siloxane suspension chains, but the mechanical properties declined to 6.8 MPa. Tang *et al.*[26]

[a]*National-Provincial Laboratory of Special Function Thin Film Materials, School of Materials Science and Engineering, Xiangtan University, Xiangtan 411105, China. E-mail: xlzhong@xtu.edu.cn, fuzhao@xtu.edu.cn*
[b]*Qingdao Green World New Material Technology Co., Ltd, Qingdao, 266100, China. E-mail: qifeng2001@126.com*

synthesized polar-group-containing side-chain extenders *via* end-controlled directed reactions. While this approach enhanced the damping properties of polyurethane elastomers, the synthesis of side-chain extenders requires strict control over drop-acceleration rates and reaction temperatures to ensure structural precision, significantly increasing the difficulty of performance regulation. Thus, how to balance the mechanical properties and damping properties of materials has become a key factor in promoting progress in this field.

5-Hydroxymethylfurfural (HMF) is a biomass platform chemical that can be efficiently synthesized through dehydration reactions from inexpensive and abundant natural resources such as corn starch and fructose, and has a structure analogous to aromatic chemicals, making HMF an intriguing research topic in high-performance polymer synthesis.[27,28] In this study, we synthesized a novel chain extender *via* Schiff base reaction, using 2,2′-diaminodiphenyl disulfide capped with HMF, and incorporated it into PUE. Meanwhile, isophorone diisocyanate (IPDI) with irregular aliphatic ring structures was introduced into the system. IPDI can disrupt the symmetry of the chain extender, forming PUE segments with active spaces, thus promoting dynamic exchange of imines, disulfide bonds, and hydrogen bonds.[7,29] In summary, PUE modified by HDF chain extension exhibits outstanding damping properties and Mechanical properties. Compared to the PUE matrix, the EDTR and tan δ area (TA) of PUE-T-HDF increased to 134 °C and 44.2 K, respectively. The tensile strength and elongation at break of PUE-HDF also improved to 19.1 MPa and 626%. Moreover, the PUE-T-HDF material has better vibration suppression performance in cantilever beam vibration tests. The molecular chain mobility of PUE was investigated through rheological, stress relaxation, and self-healing experiments. Overall, we anticipate that this research will further advance the application of 5-hydroxymethylfuran in the fields of vibration and noise reduction.

2. Experimental

2.1 Materials

Toluene diisocyanate (2,4-TDI, NCO% = 48.2) and Isophorone diisocyanate (IPDI, NCO% = 37.5) were both purchased from Yantai Wanhua Chemical Group Co., Ltd (China). 5-Hydroxymethylfurfural (HMF), 2,2′-diaminodiphenyl disulfide (2-DAPS, AR), and methanol (LC) were all supplied by Shanghai MacLean Biochemical Technology Co., Ltd (China). Polyethylene glycol propylene glycol adipate (PEPA2000, M_n = 2000) was purchased from Yantai Huada Chemical Industry Co., Ltd (China). Dibutyltin dilaurate (DBTDL), *N*,*N*-dimethylformamide (DMF, AR), and trimethylolpropane (TMP, AR) were purchased from Shanghai Aladdin Co., Ltd (China).

2.2 Synthesis of PUE

2.2.1 Synthesis of HDF. First, place the measured amount of 2-DAPS into a three-neck flask containing 50 mL of methanol and heat to 40 °C until completely dissolved. Then, slowly add HMF dropwise to the aforementioned solution after dissolving it in 50 mL of methanol (molar ratio of HMF to 2-DAPS: 2 : 1). The mixture is thoroughly mixed, heated to 60 °C, and then refluxed for 6 h under nitrogen. After the reaction, the solvent was removed by rotary evaporation to afford the crude product, which was then purified by cold recrystallization to yield the target compound (HDF) in 83% yield.

2.2.2 Synthesis of prepolymers. First, add metered amounts of PEPA2000 to a three-neck flask. Under vacuum conditions of −0.1 MPa and a temperature of 110–120 °C, perform water removal treatment for 2–3 h until no water vapor condenses on the inner walls of the three-neck flask, completing the pretreatment. TDI was then added in the required amount, and the reaction temperature was maintained at 70–80 °C. The mixture was allowed to react at this temperature for 2.5 h. During the reaction, the isocyanate (NCO) content was monitored by hydrochloric acid-dibutylamine titration. The reaction was terminated when the NCO content reached 6%, and the resulting prepolymer was sealed and stored for subsequent use.

2.2.3 Chain expansion and forming. First, calculate the amount of IPDI to be added to adjust the total NCO content in the system from 6% to 8%. Measured amounts of IPDI, prepolymer, HDF, and DMA are first added to a three-necked flask, followed by a single drop of dibutyltin dilaurate (DBTDL). The mixture is stirred thoroughly, and after reacting for 1 h, the "preliminary chain extended product" is obtained. Then, add the TMP to the preliminary chain extended product, stir rapidly to achieve uniform mixing, and then quickly pour the mixture into a PTFE mold. Transfer the mold to a vacuum drying oven maintained at 60 °C, evacuate to a vacuum of −0.1 MPa, and degas for 30 min. Once no bubbles are visible in the flask, raise the temperature to 80 °C and cure for 16 h. The PUE produced were named according to the different molar ratios of HDF and TMP: PUE-TMP, PUE-T-5HDF, PUE-T-10HDF, PUE-T-15HDF, and PUE-T-20HDF. PUE-TMP indicates zero content of HDF, PUE-T-5HDF means 5% HDF, with subsequent designations following this pattern. Additionally, comparative sample PUE-T-20SS indicates that the molar fraction of 2-DAPS in the chain extender is 20%. This sample was prepared using the same method as PUE-T-20HDF, except that the HDF in the chain extender was replaced with 2-DAPS. The specific reaction process and experimental formulation are illustrated in Fig. 1 and Table S1:

2.3 Characterization

Infrared spectroscopy testing was performed using a Fourier Transform Infrared (FTIR) Spectrometer (Nicolet iS5, USA) within the scanning range of 400–4000 cm^{-1}. The spectral resolution was set to 4 cm^{-1}.

The chemical composition of the chain extender (HDF) was studied by nuclear magnetic resonance (NMR) hydrogen spectroscopy (Avance III 400 MHz, Bruker, Germany) under conditions of 16 scans and deuterated DMSO as the solvent.

To investigate the crystal structure of polyurethane and its composite materials, experiments were conducted using a

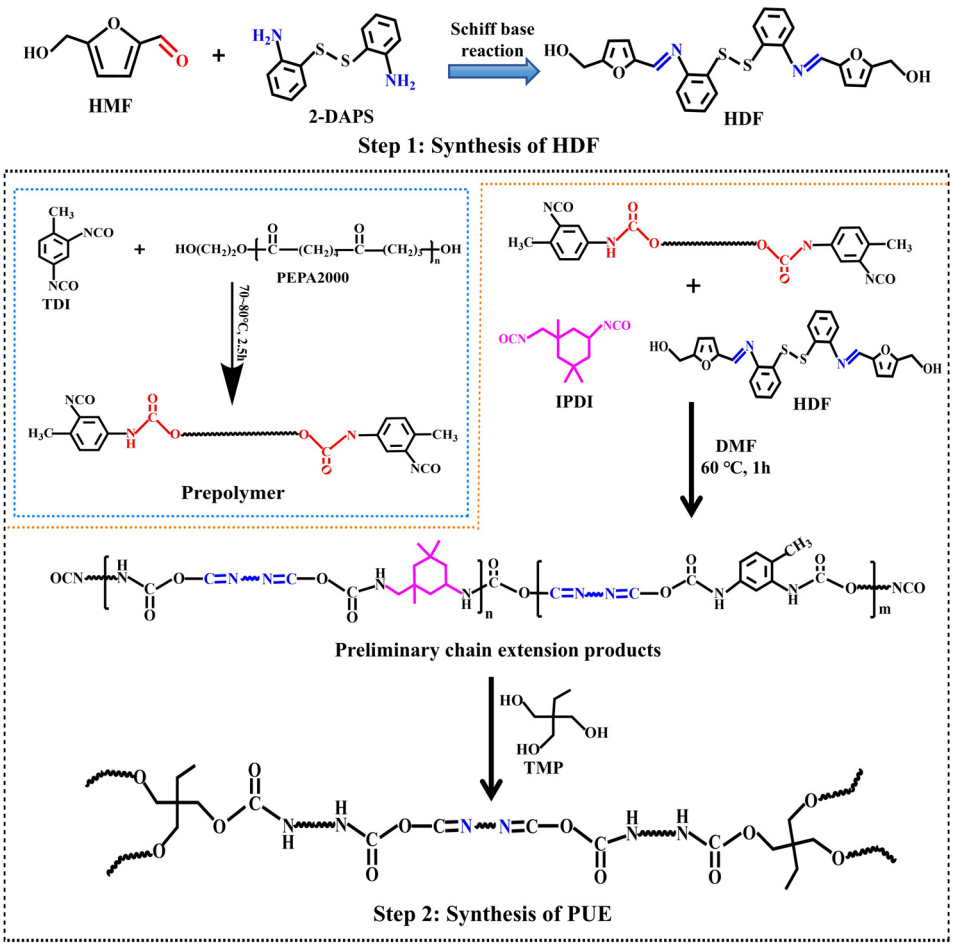

Fig. 1 Schematic diagram of PUE-T-HDF preparation.

SmartLab SE X-ray diffractometer (XRD) as the light source. Testing was performed with a scanning range of 5–90° and a scanning rate of 10° min^{-1}.

According to the GB/T 18258-2000 standard, use a self-assembled resonance test system to carry out vibration measurement on the sample.

The incorporation of dynamic disulfide bonds was confirmed within the wavenumber range of 300–1700 cm^{-1} using Raman spectroscopy (Horiba LabRAM HR Evolution, 785 nm).

Thermogravimetric analysis (TGA) of PUE samples was conducted using a Q500 instrument manufactured by TA Instruments under nitrogen purging conditions. The specific procedure involved heating the samples from 30 °C to 600 °C at a heating rate of 10 °C min^{-1}.

In accordance with the GB/T 528-2009, tensile tests were conducted on the samples using a Tensile Testing Machine (WDW-100C). A total of three tests were performed, and the results were averaged.

The thermodynamic properties testing was conducted using a dynamic thermal mechanical (DMA) analyzer manufactured by the German company KBA. The tests were performed in tensile mode, employing a temperature range of −80 °C to 120 °C with a heating rate of 2 °C min^{-1} and a constant frequency of 10 Hz.

The rheological performance of the sample was tested utilizing a Haake Mars40 rheometer under the following conditions: fixed strain mode, strain rate of 1.5%, and a frequency scan range of 0.1–100 rad s^{-1}.

The self-healing behavior of the sample was examined under an optical microscope. The self-healing efficiency is defined as:

$$\eta = \frac{\sigma_{\text{healed}}}{\sigma_{\text{pristine}}}$$

Among these, σ_{healed} denotes the tensile strength after repair, while σ_{pristine} represents the tensile strength of the original sample.

3. Results and discussion

3.1 Material characterization

To verify the successful synthesis of the novel chain extender (HDF) shown in Fig. 1, the prepared product was subjected to

FTIR, ^{1}H NMR, and Raman spectroscopy analysis. As shown in Fig. 2a, in the HDF Spectrogram, the characteristic absorption peak of the N–H stretching vibration absorption band of 2-DAPS (3300–3400 cm^{-1}) and the aldehyde group corresponding to HMF at 1674 cm^{-1} have both essentially disappeared. Meanwhile, a newly observed absorption peak at 1624 cm^{-1} is ascribed to the stretching vibration of the imine bond (C=N).[30] This shift provides direct evidence for the formation of HDF through the condensation reaction between HMF and 2-DAPS. Fig. 2b presents the ^{1}H NMR spectrum of HDF. The residual DMSO-d$_6$ solvent peak appears at δ 2.50 ppm. Benzene-ring proton signals occur between δ 7.16 and 7.54 ppm, while the resonances at δ 6.53 and 6.71 ppm are allocated to distinct furan-ring protons. Furthermore, the peak at δ 8.45 ppm is attributed to the imine proton formed by the condensation of HMF with 2-DAPS. The characteristic proton peak of the imine group is in agreement with the FTIR of HDF in Fig. 2a, further confirming the successful synthesis of the HDF Schiff base. Additionally, the Raman spectra of 2-DAPS and HDF are displayed in Fig. 2c. It is found that characteristic Raman peaks of the S–S bond and C–S bond appear at 510 cm^{-1} and 670 cm^{-1} in HDF, indicating the successful incorporation of dynamic disulfide bonds into HDF.[22]

In addition, FTIR characterization was performed on the raw materials and PUE materials. As shown in Fig. 2d, compared to the FTIR spectrum of TDI, the intensity of the characteristic –NCO peak (2271 cm^{-1}) in the prepolymer was significantly reduced. Meanwhile, the characteristic peaks appearing at 3348 cm^{-1} and 1727 cm^{-1} corresponded to N–H and C=O stretching vibrations, respectively, indicating the successful formation of urethane bonds. Compared to the prepolymer, the –NCO group absorption peak at 2271 cm^{-1} in the PUE has completely disappeared, suggesting that the chain extender has fully reacted with the prepolymer.[31] To investigate the effect of HDF introduction on hydrogen bonding, peak-fitting analysis was performed on the C=O stretching vibration region (1550–1780 cm^{-1}) for PUE-TMP, PUE-T-20SS, and PUE-T-20HDF. As seen in Fig. 1e, the C=O absorption band of PUE-T-20HDF can be divided into four sub-peaks. These sub-peaks correspond to disordered hydrogen-bonded C=O (1678 cm^{-1}), free hydrogen-bonded C=O (1731 cm^{-1}) and ordered hydrogen-bonded C=O (1600 and 1711 cm^{-1}). The hydrogen-bonded C=O content was evaluated *via* the ratio of the sum of peak areas at 1600 cm^{-1}, 1678 cm^{-1}, and 1711 cm^{-1} to the total carbonyl peak area.[29] Results indicate that the hydrogen bond C=O content of PUE-T-20HDF reached 83.1%, which was 2.7% and 12.4% greater than that of PUE-TMP and PUE-T-20SS, respectively (Fig. S1 and Table S2). In addition, as shown in Fig. S2, with increasing HDF content, the carbonyl absorption band of PUE near 1734 cm^{-1} gradually shifted toward lower wavenumbers, further indicating enhanced hydrogen-bonding interactions in the system.[32] As shown in the XRD pattern in Fig. S3, all samples exhibit an amorphous structure. Compared to PUE-TMP, PUE-T-20HDF has lower peak intensity and broader peak shapes. This may be attributed to the irregular structure

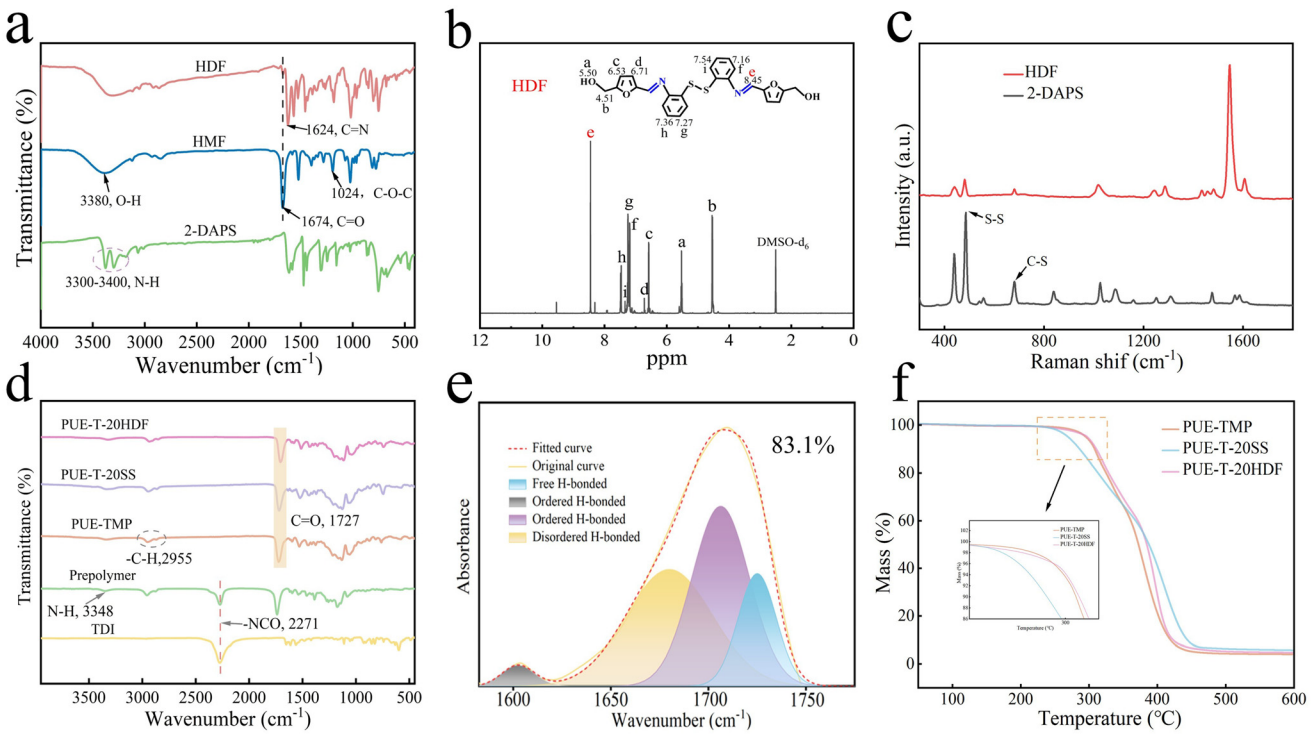

Fig. 2 (a) FTIR spectra of HMF, 2-DAPS, and HDF. (b) ^{1}H NMR spectrum of HDF. (c) Raman spectra of 2-DAPS and HDF. (d) FTIR spectra of PUE. (e) Peak fitting of the carbonyl peak in PUE-T-20HDF. (f) TG curves of PUE-TMP, PUE-T-20SS, and PUE-T-20HDF.

of IPDI and the reversible dynamic bonds, which increase disorder within the system.[33]

As shown in the TG curve in Fig. 2f, the initial decomposition temperature and T_5 of PUE-T-20SS are both lower than those of PUE-TMP. This is primarily attributable to the relatively lower bond energy of the dynamic disulfide bonds, whose preferential cleavage precipitates the premature onset of thermal decomposition in the material.[34]

Meanwhile, the T_5 and initial decomposition temperature of PUE-T-20HDF are similar to those of PUE-TMP. The DTG curve in Fig. S4 indicates that the thermal degradation of PUE occurs in two stages. The shoulder peak at 280–330 °C corresponds to the thermal degradation of hard segments containing urethane groups, and the peak at 370–420 °C is due to the degradation of the soft segment polyester chains and chain extenders.[35] PUE-T-20HDF achieved a maximum pyrolysis temperature (T_{max}) of 399.4 °C and a higher char yield (Table S3). This improvement may be attributed to the rigid furan/benzene ring structures in the HDF chain extender, thereby enhancing the thermal stability of PUE.[36]

3.2 Damping performance analysis

To analyze the damping properties of PUE materials at different temperatures, dynamic mechanical testing was utilized. The tan δ is a critical indicator for assessing the damping properties of materials. Typically, the temperature corresponding to tan δ > 0.3 is referred to as the effective damping temperature range (EDTR).[37] Detailed damping performance parameters are shown in Table S4. The damping properties of PUE significantly improve with increasing HDF content. When the HDF content reached 20%, the material exhibited optimal damping performance. The EDTR expanded from 38 °C for PUE-TMP to 134 °C for PUE-T-20HDF, and the tan δ_{max} increased from 1.05 to 1.38 (Fig. 3a and b). Additionally, the TA is defined as the integrated area of the tan δ–T curve within the temperature range where tan $\delta \geq 0.3$, expressed as $TA = \int_{T_1}^{T_2} \tan \delta dT$, where T_1 and T_2 are initial and final temperature of damping temperature range where tan δ is greater than or equal to 0.3.[29] The TA value comprehensively reflects the energy dissipation capability of the PUE material (Fig. S5). As shown in Fig. 3c, the TA value of PUE-T-20HDF was 44.2 K, improving by 277% compared to PUE-TMP. The enhanced damping performance is mainly attributed to the reversible hydrogen-bonding interactions, together with the dynamic exchange of disulfide and imine bonds, which provide multiple energy dissipation pathways for the PUE network.[38] These results are jointly influenced by the storage modulus (E') and loss modulus (E''). As shown in Fig. 3d, all samples exhibit relatively high E' values in the glassy region. With increasing temperature, the gradual unfreezing of polymer chain segments leads to a marked decrease in E'. Meanwhile, the thermally activated dynamic exchange of disulfide and imine bonds promotes chain mobility and network rearrangement. As shown in Fig. S6, PUE-T-20HDF

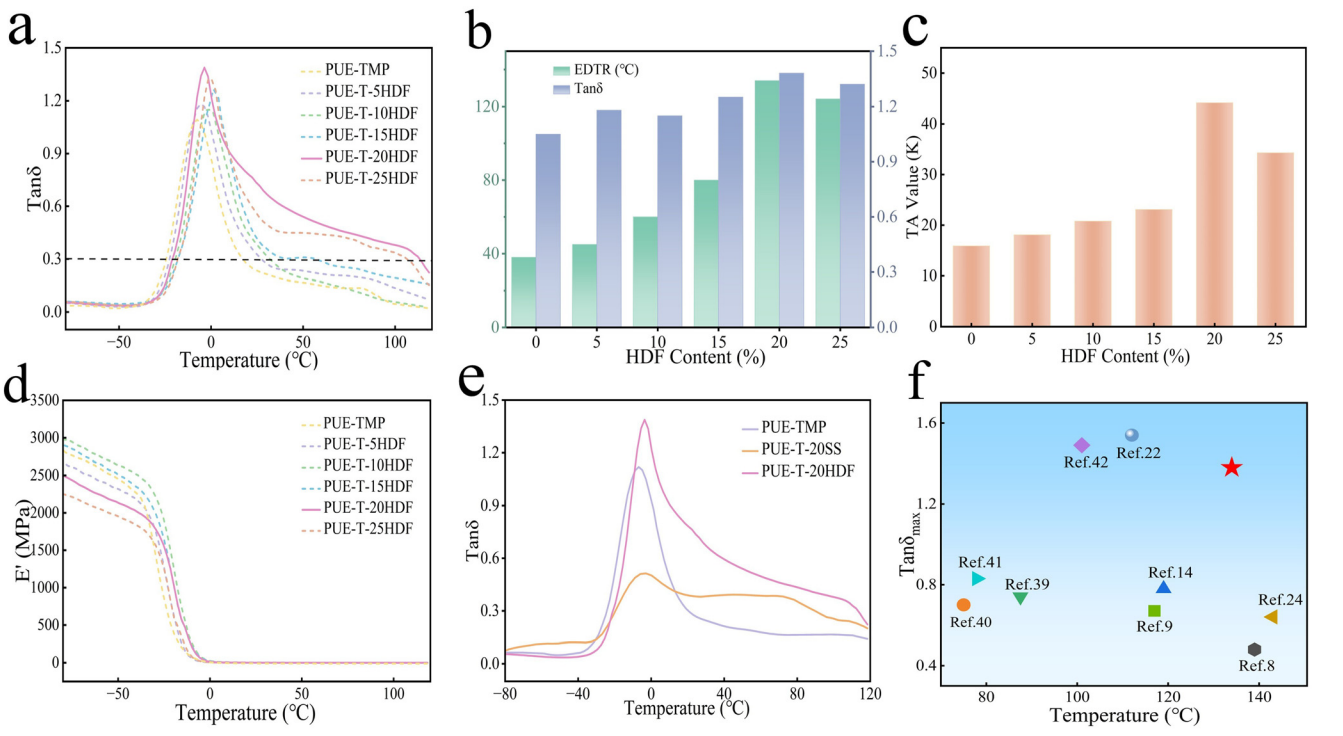

Fig. 3 (a) Loss factor-temperature curve. (b) EDTA and tan δ variation trend diagram. (c) TA value comparison. (d) Energy storage modulus curve. (e) Damping performance comparison of PUE-TMP, PUE-T-20SS, and PUE-T-20HDF. (f) Damping performance comparison of PUE materials from different literature sources.[8,9,14,22,23,39–42]

maintains a relatively high E'' over a broad temperature range, indicating its superior energy dissipation capability. As shown in Fig. 3e and f, PUE-T-20HDF demonstrates significant advantages in both EDTR and tan δ_{max}, confirming the effectiveness of this research strategy in enhancing the damping properties of the material.

3.3 Mechanical properties analysis

The tensile strength and elongation at break of PUE with different HDF contents are shown in Fig. 4 and Table S5. The elongation at break of PUE increased from 326% to 680% as the HDF content increased. Meanwhile, compared with PUE-TMP, the tensile strength of samples containing 0–20% HDF showed some fluctuation but no monotonic downward trend. At 20% HDF content, the tensile strength and elongation at break of PUE-T-20HDF were 19.1 MPa and 626%, respectively, demonstrating a relatively balanced of strength and elongation. However, when the HDF content was further increased to 25%, the tensile strength decreased to 12.4 MPa, possibly due to the excessive incorporation of dynamic bonds, which promoted chain mobility and network relaxation.[43] Additionally, as shown in Fig. S7, the variation in PUE hardness is consistent with the trends observed in the mechanical tests. Therefore, PUE-T-20HDF was selected for subsequent study because it showed the best overall balance between mechanical and damping properties.

3.4 Molecular chain movement analysis

Unlike fixed crosslinked networks, dynamic bonds can reconfigure the molecular network structure of materials through reversible breakage and recombination. To investigate the molecular chain mobility of PUE materials, we employed rheological testing, stress relaxation, and self-healing experiments for characterization. As shown in Fig. 5a and Fig. S8, the rheology of PUE-TMP, PUE-T-20SS and PUE-T-20HDF was measured at 100 °C, 120 °C, and 140 °C. For PUE-TMP, G' was larger than G'' for the whole frequency region. This is primarily attributed to the stable three-dimensional network formed by PUE after TMP chain extension, which severely restricts segment motion. Compared to PUE-T-20SS, PUE-T-20HDF exhibits a G'–G'' crosspoint at 120 °C, marking the shift from a dominant elastic behavior ($G' > G''$) to a dominant viscous ($G' < G''$).[44] The crossover frequency, ω_c, is generally defined as the characteristic relaxation frequency of the material, and the corresponding characteristic relaxation time can be estimated by $\tau_c = 1/\omega_c$.[45] PUE-T-20HDF exhibits the G'–G'' crossover at 120 °C and a shorter characteristic relaxation time at the same temperature (140 °C), indicating that network rearrangement and stress relaxation occur more readily in this system at high temperature.

The stress relaxation behavior of the PUE materials was tested at 80 °C using a dynamic thermal mechanical analyzer. The relaxation time is the time required for the modulus to relax to its initial value of 1/e. which directly reflects the strength of molecular chain motion and rearrangement capability.[46] As indicated in Fig. 5b, PUE-T-20HDF had the shortest relaxation time (5.1 min), followed by PUE-T-20SS (15.2 min), while PUE-TMP failed to reach a determinable relaxation time. The relaxation time of PUE shortens significantly with the introduction of dynamic bonds, consistent with the rheological test. This confirms that the introduction of HDF can effectively enhance the motion and rearrangement of PUE molecular chains. To further study the molecular chain motion of PUE, scratch repair tests for PUE-TMP, PUE-T-20SS, and PUE-T-20HDF are performed with a surgical blade. As shown in Fig. 5c, PUE-T-20HDF displays superior self-healing properties, with its surface scratches healing after 3 h at 80 °C. As depicted in Fig. 5d, a 0.4934 g sample of PUE-T-20HDF was cut and heated at 120 °C for 2 h. The repaired sample withstood a 1 kg load without fracture, demonstrating a load-bearing capacity approximately 2028 times its own weight. In addition, as shown in Fig. S9, the cut PUE-T-20HDF specimens were subjected to tensile testing after self-healing at 80 °C for 12 h. The results showed that the tensile strength recovered to 83.7% of that of the original sample. The exceptional self-healing properties of PUE-T-20HDF stem primarily from two factors. First, the disulfide bonds and imine bonds within the PUE chain segments undergo reversible dynamic exchange at specific

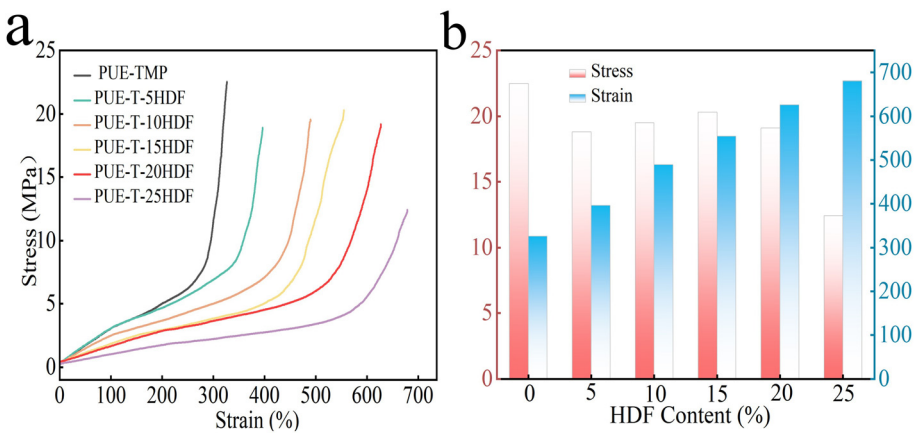

Fig. 4 Effect of HDF content on the mechanical properties of PUE.

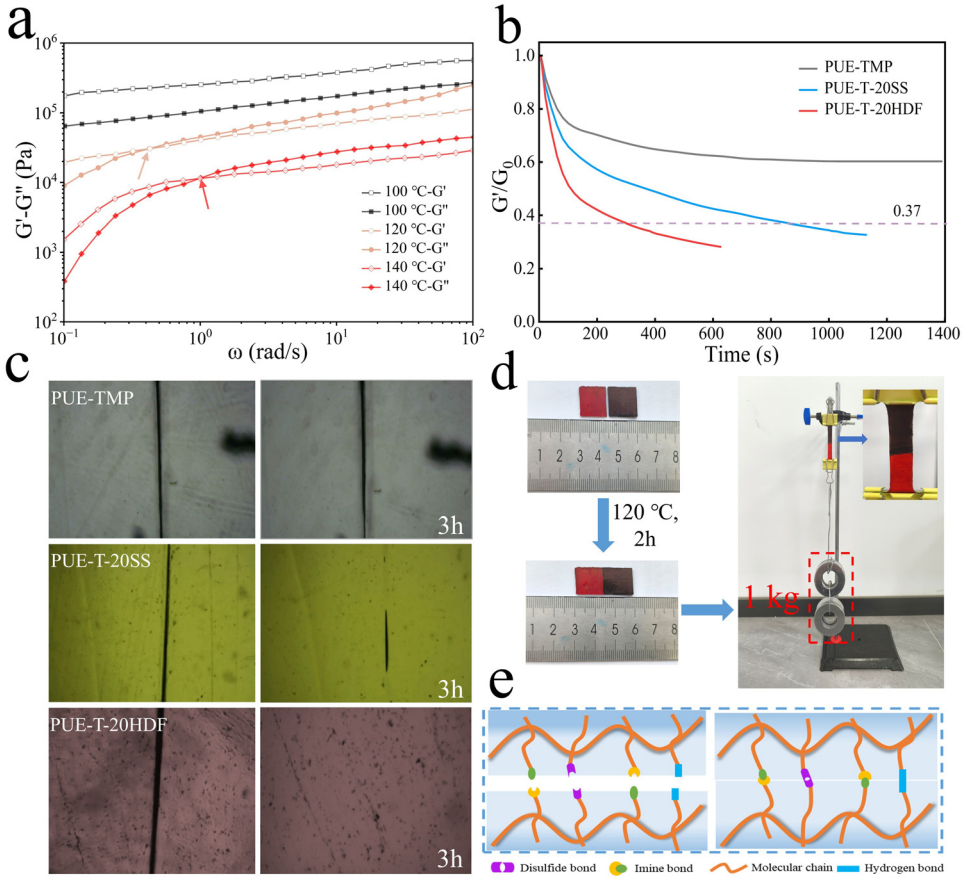

Fig. 5 (a) Rheological properties of PUE-T-20HDF. (b) Stress relaxation curves of three different PUE. (c) Scratch self-healing images of PUE-TMP, PUE-T-20SS, and PUE-T-20HDF at 80 °C. (d) Self-healing performance of PUE-T-20HDF at 120 °C. (e) Schematic of the self-healing mechanism for PUE-T-20HDF.

temperatures. Second, hydrogen bonding interactions form between the urethane groups along the molecular chains. The combination of these two mechanisms endows the material with outstanding self-repair capabilities (Fig. 5e).[47] Notably, this self-healing behavior is consistent with the aforementioned damping results, indicating that dynamic reversible bond exchange can not only promote energy dissipation through bond breaking and reformation, thereby enhancing the damping performance of the PUE material, but also promote network reconstruction and endow the material with self-healing capability.

3.5 Vibration performance analysis

To evaluate the vibration damping performance of PUE materials in practical applications, this section presents vibration tests and ball-drop tests conducted on PUE-TMP, PUE-T-20SS, and PUE-T-20HDF. Fig. S10 illustrates the schematic diagram of measuring material vibration damping performance using the resonance method. The test procedure is as follows: first, secure the PUE strip (150 mm × 10 mm × 1 mm) to a steel bar of 1 mm thickness to form a composite cantilever beam. Subsequently, a signal generated by the signal source and amplified by the power amplifier drives the exciter to apply excitation to the free end of the steel bar. The vibration acceleration of the composite cantilever beam is collected and recorded by the acceleration sensor at its end. By analyzing the vibration acceleration–time curve, the vibration properties of materials can be evaluated. Compared to PUE-TMP (0.44 $mm^2\ s^{-1}$), the initial vibration accelerations of PUE-T-20SS and PUE-T-20HDF were reduced by 0.36 $mm^2\ s^{-1}$ and 0.25 $mm^2\ s^{-1}$, respectively (Fig. 6a). Additionally, the overall acceleration–time curve shows that the PUE-T-20HDF has excellent vibration damping performance, with its acceleration gradually stabilizing after 6 s. The drop ball test results are displayed in Fig. 6b, Fig. S11 and Videos, where a 43 g steel ball was dropped freely from a height of 1 m. When the surface contained no sample material or only PUE-T-20SS, the ball rebounded to heights of 57 cm and 15 cm, respectively. However, when 1.2 mm thick PU-T-20HDF was added, the rebound height was reduced to 2.5 cm. To further assess the protective properties of PUE, slide glass experiments were carried out on PUE-TMP, PUE-T-20SS, and PUE-T-20HDF. It can be observed from Fig. 6c that only the slide glass protected by PUE-T-20HDF did not break. The results above indicate that the PUE-T-20HDF displays exceptional vibration damping performance due to its multiple dynamic bond structures that

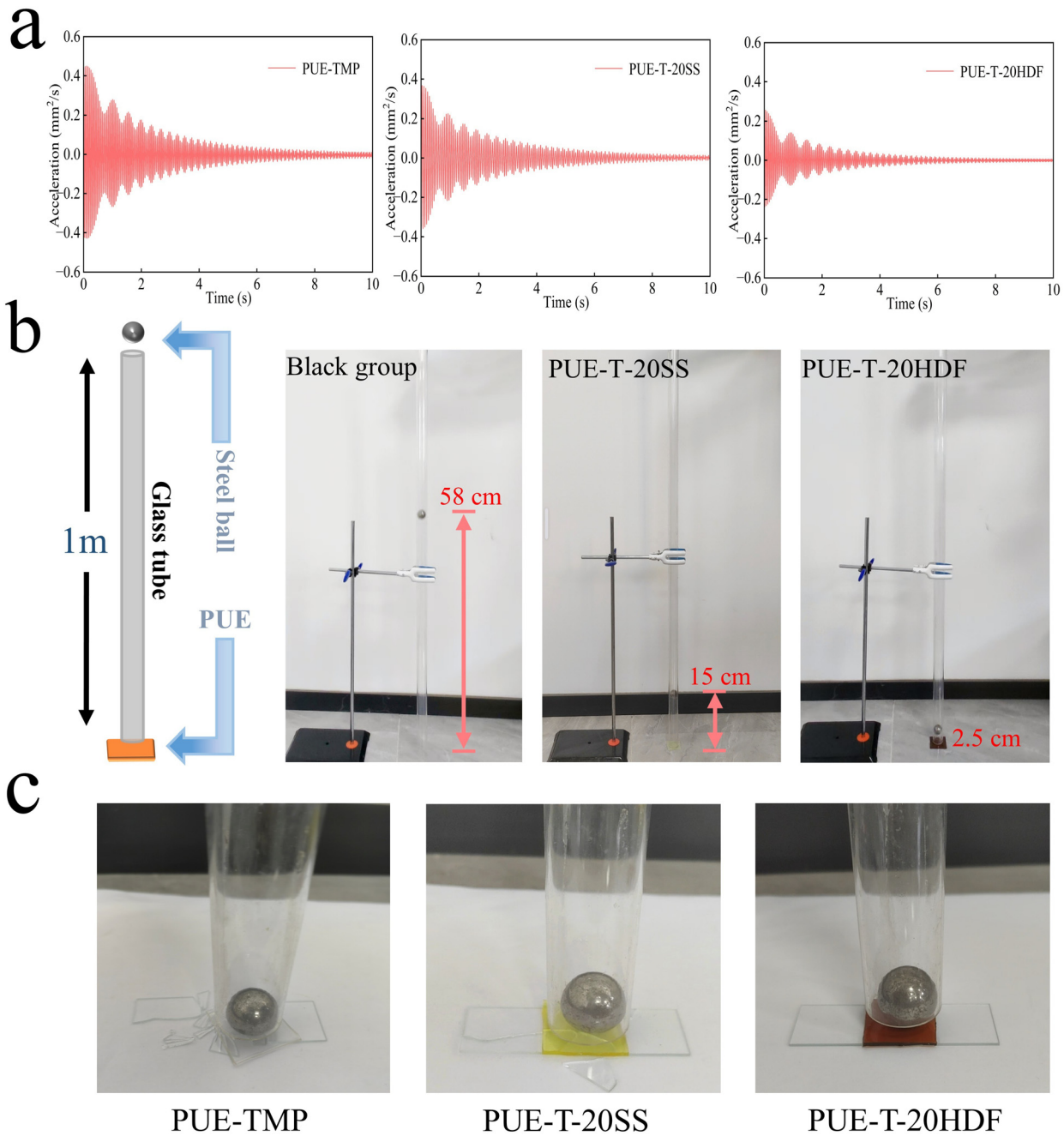

Fig. 6 (a) Acceleration–time curves for PUE-TMP, PUE-T-20SS, and PUE-T-20HDF. (b) Drop ball rebound test. (c) Slide impact test.

efficiently dissipate energy. Consequently, it is particularly suitable for applications such as vibration damping supports for precision instruments and isolation/soundproofing bases for high-end audio equipment.

3.6 Damping mechanism analysis

DMA results indicate that HDF can effectively enhance the damping performance of PUE. The improved energy dissipation is mainly attributed to the introduction of the HDF chain extender, which incorporates dynamic disulfide and imine bonds into the PUE network. Under external stimuli, these dynamic bonds dissipate energy through reversible dissociation and recombination, while also promoting segmental motion of the polymer chains. The enhanced chain mobility increases the opportunities for polar groups, such as –NH– and C═O, to associate and dissociate, thereby facilitating the dynamic breaking and reformation of the hydrogen-bonding network (Fig. 7 and Fig. S12). Therefore, the combined effect of dynamic disulfide bonds, imine bonds, and hydrogen bonding networks is a key factor in enhancing the damping performance of PUE and broadening its effective damping temperature range.

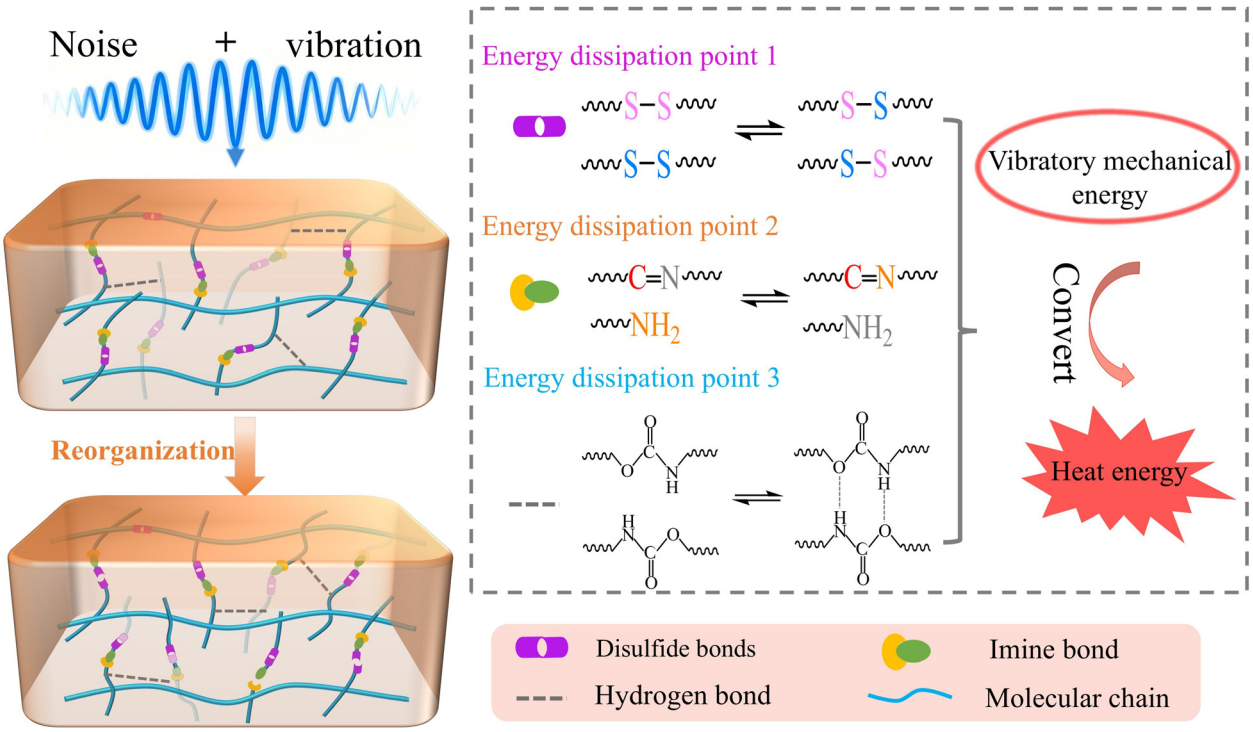

Fig. 7 Diagram of the damping mechanism of the PUE-T-20HDF.

4. Conclusion

In this work, we synthesized a novel chain extender (HDF) featuring disulfide and imine bonds by using HMF-terminated 2-DAPS derived from a biomass platform, and incorporated it into PUE in combination with IPDI. The incorporation of HDF and IPDI endows PUE materials with outstanding damping performance. This is mainly contributed by the reversible dynamic exchange of disulfide bonds, imine bonds, and hydrogen bonds at specific temperatures, as well as the irregular aliphatic ring structure of IPDI disrupting the symmetry of PUE molecular chains, synergistically enhancing the energy dissipation capability of the material. Compared to PUE-TMP, the EDTR and $\tan\delta_{max}$ of PUE-T-20HDF reached 134 °C (−19 °C to 115 °C) and 1.38, respectively. Meanwhile, cantilever beams coated with PUE-T-20HDF demonstrate exceptional amplitude attenuation ability. Additionally, PUE-T-20HDF possesses a tensile strength of 19.1 MPa and an elongation at break of 626%, while displaying remarkable self-healing ability at 80 °C. We anticipate that this research will provide new insights and foster the broader adoption of dynamic bonds in the field of damping.

Author contributions

Shaolong Li: experimental operation, writing – original draft, data curation, formal analysis, investigation. Chunyang Di: supervision, conceptualization. Yongpeng Yang: validation, investigation. Yang Zhao: investigation, formal analysis. Yutong Li: validation, investigation. Hongjia Song: validation, supervision. Jinbin Wang: funding acquisition, validation, supervision. Feng Qi, Zhao Fu and Xiangli Zhong: funding acquisition, writing – review & editing, supervision, project administration, validation.

Conflicts of interest

The authors declare no conflict of interest.

Data availability

The data supporting this article have been included as part of the supplementary information (SI). Supplementary information is available. The supplementary information includes detailed data sheets on damping and mechanical properties, as well as further experimental details, including Fourier-transform infrared spectroscopy (FTIR), X-ray diffraction (XRD), rheological testing, and drop ball testing. See DOI: https://doi.org/10.1039/d6lp00009f.

Acknowledgements

This research was funded by the National Natural Science Foundation of China (No. 12505329, 52472139, 12275230).

References

1 S. Hu, Y. Wu, G. Fu, *et al.*, Bio-Based Polyurethane and Its Composites towards High Damping Properties, *Int. J. Mol. Sci.*, 2022, **23**(12), 6618.
2 Z. Qiao, J. Xiao and L. Xun, A multi-functional polyurethane elastomer with high damping, water resistance and flame retardancy, *React. Funct. Polym.*, 2024, **196**, 105838.
3 X. Zhao, R. Jin, Z. Niu, *et al.*, Fabrication of Polyurethane Elastomer/Hindered Phenol Composites with Tunable Damping Property, *Int. J. Mol. Sci.*, 2023, **24**(5), 4662.
4 Z. Gou, S. Zhang, W. Zhu, *et al.*, Improving friction vibration and noise characteristics of carbon fiber-reinforced resin composites by utilizing Polyurethane's enhanced damping capacity, *Compos. Commun.*, 2025, **57**, 102492.
5 J. Ma, C. Ma, R. Long, *et al.*, Effect of Hard-Segment Structure on the Properties of Polyurethane/Poly (Ethyl Methacrylate) Damping Composites, *Polymers*, 2025, **17**(5), 63.
6 X. Zhao, G. Fu, Y. Wang, *et al.*, Bio-based polyurethane/hindered phenol AO-80 composites for room temperature high damping properties, *Composites, Part B*, 2022, **243**, 110118.
7 D. Wang, Z. Wang, S. Ren, *et al.*, Molecular engineering of a colorless, extremely tough, superiorly self-recoverable, and healable poly(urethane-urea) elastomer for impact-resistant applications, *Mater. Horiz.*, 2021, **8**(8), 2238–2250.
8 F. Wang, Y. Zhu, L. Wang, *et al.*, The facile and effective approach for fabricating polyurethane gradient materials with significant damping properties, *J. Appl. Polym. Sci.*, 2023, **140**(47), e54708.
9 X. Lv, Z. Huang, C. Huang, *et al.*, Damping properties and the morphology analysis of the polyurethane/epoxy continuous gradient IPN materials, *Composites, Part B*, 2016, **88**, 139–149.
10 N. Babkina, O. Antonenko, L. Kosyanchuk, *et al.*, Effect of polyurethane material design on damping ability, *Polym. Adv. Technol.*, 2023, **34**(11), 3426–3437.
11 K. Shi, X. Li, L. Lei, *et al.*, Influence of dangling chains on the microphase separation and damping properties of polyurethane, *J. Appl. Polym. Sci.*, 2024, **141**(34), E55867.
12 X. Tang, X. Guo, L. Gong, *et al.*, Microstructure construction design and damping properties of polyurethane microporous elastomer modified by suspension chain extender via end-controlling oriented synthesis, *Polymer*, 2023, **270**, 125748.
13 J. Zhou, H. Li and X. Lu, Damping elastomer with broad temperature range based on irregular networks containing hyperbranched polyester and dangling chains, *Polym. Adv. Technol.*, 2018, **29**(8), 2308–2316.
14 Q. Feng, M. Shen, J. Zhu, *et al.*, Realization of polyurethane/epoxy interpenetrating polymer networks with a broad high-damping temperature range using β-cyclodextrins as chain extenders, *Mater. Des.*, 2021, **212**, 110208.
15 X. Li, Y. Niu, T. Ai, *et al.*, Preparation and Performance Study of Polyurethane/Epoxy Resin Interpenetrating Networks with Self–Healing, Shape Memory, and High Damping Properties, *Macromol. Chem. Phys.*, 2023, **225**(1), 2300311.
16 J. Sethi, M. Illikainen, M. Sain, *et al.*, Polylactic acid/polyurethane blend reinforced with cellulose nanocrystals with semi-interpenetrating polymer network (S-IPN) structure, *Eur. Polym. J.*, 2017, **86**, 188–199.
17 W. Chen, X. Lu, Q. Zheng, *et al.*, Interface Optimizing Core-Shell PZT@Carbon/Polyurethane Composites with Enhanced Passive Piezoelectric Vibration Damping Performance, *ACS Appl. Mater. Interfaces*, 2024, **16**(6), 7742–7753.
18 W. Lei, C. Fang, X. Zhou, *et al.*, Polyurethane elastomer composites reinforced with waste natural cellulosic fibers from office paper in thermal properties, *Carbohydr. Polym.*, 2018, **197**, 385–394.
19 J. Zheng, S. Sun, X. Hu, *et al.*, Ultra–Damping Composites Enhanced by Yolk-Shell Piezoelectric Damping Mechanism, *Adv. Funct. Mater.*, 2023, **33**(15), 2213343.
20 Z. Shi, J. Kang and L. Zhang, Water-Enabled Room-Temperature Self-Healing and Recyclable Polyurea Materials with Super-Strong Strength, Toughness, and Large Stretchability, *ACS Appl. Mater. Interfaces*, 2020, **12**(20), 23484–23493.
21 Z. Zhang, X. Jiang, Y. Ma, *et al.*, High-Performance Branched Polymer Elastomer Based on a Topological Network Structure and Dynamic Bonding, *ACS Appl. Mater. Interfaces*, 2023, **15**(36), 43048–43059.
22 G. Dong, Y. Chang, C. Li, *et al.*, Study on damping and self–healing properties of polyurethane materials based on dynamic synergetic control of disulfide bond and imine bond, *J. Appl. Polym. Sci.*, 2023, **140**(42), e54544.
23 Y. Ma, R. Qin, M. Xu, *et al.*, Wide temperature range damping polyurethane elastomer based on dynamic disulfide bonds, *J. Appl. Polym. Sci.*, 2021, **139**(2), 51453.
24 H. Rong, M. Xu, X. Jiang, *et al.*, Synthesis and molecular dynamics study of high-damping polyurethane elastomers based on the synergistic effect of dangling chains and dynamic bonds, *Polym. Chem.*, 2022, **13**(29), 4260–4272.
25 J. Xiao, Q. Rui, W. Min, *et al.*, Controllable wide temperature range and high damping polyurethane elastomer based on disulfide bond and dangling chain, *Polym. Adv. Technol.*, 2021, **32**(5), 2185–2196.
26 X. Tang, X. Guo, X. Liu, *et al.*, Self-healing polyurethane elastomer with wider damping temperature range by synergistic interaction of suspended chains and dynamic disulfide bonds, *Polym. Test.*, 2023, **124**, 108070.
27 M. Sayed, N. Warlin, C. Hulteberg, *et al.*, 5-Hydroxymethylfurfural from fructose: an efficient continuous process in a water-dimethyl carbonate biphasic system with high yield product recovery, *Green Chem.*, 2020, **22**(16), 5402–5413.
28 N. Warlin, M. Garcia, S. Mankar, *et al.*, A rigid spirocyclic diol from fructose-based 5-hydroxymethylfurfural: syn-

thesis, life-cycle assessment, and polymerization for renewable polyesters and poly(urethane-urea), *Green Chem.*, 2019, **21**(24), 6667–6684.

29 Y. Qin, F. Qi, C. Di, *et al.*, Ultra-wide damping temperature range polyurethane elastomer enabled by an asymmetrically structured chain extender with double disulfide bonds, *J. Mater. Res. Technol.*, 2024, **29**, 2097–2107.

30 S. Lee, S. Shin and D. Lee, Self-healing of cross-linked PU via dual-dynamic covalent bonds of a Schiff base from cystine and vanillin, *Mater. Des.*, 2019, **172**, 107774.

31 H. Wu, H. Xie, X. Tian, *et al.*, Hard, tough and fast self-healing thermoplastic polyurethane, *Prog. Org. Coat.*, 2021, **159**, 106409.

32 D. Yin, Y. Liu, X. Wang, *et al.*, Novel bio-based polyurethane elastomers for adjustable room-temperature damping property, *Compos. Commun.*, 2024, **49**, 101975.

33 Z. Cui, Y. Zhang, N. Li, *et al.*, Hybrid dynamically cross-linked polyurethanes with room temperature self-healing ability for light-responsive actuator, *Mater. Today Chem.*, 2024, **42**, 102427.

34 W. Xia, B. Sun, Y. He, *et al.*, Effect of disulfide bond content on thermal-healing properties of castor oil-based polyurethanes, *Polym. Degrad. Stab.*, 2024, **229**, 110943.

35 P. Parcheta, E. Głowińska and J. Datta, Effect of bio-based components on the chemical structure, thermal stability and mechanical properties of green thermoplastic polyurethane elastomers, *Eur. Polym. J.*, 2020, **123**, 109422.

36 M. Piątek-Hnat, A. Bielawska-Pohl, *et al.*, Effect of Aromatic Chain Extenders on Polyurea and Polyurethane Coatings Designed for Defense Applications, *Polymers*, 2023, **15**(3), 756.

37 S. Park, S. Cho, H. Seo, *et al.*, Natural cork agglomerate enabled mechanically robust rigid polyurethane foams with outstanding viscoelastic damping properties, *Polymer*, 2021, **217**, 123437.

38 J. Xiao, X. Min, W. Minhui, *et al.*, Preparation and molecular dynamics study of polyurethane damping elastomer containing dynamic disulfide bond and multiple hydrogen bond, *Eur. Polym. J.*, 2022, **162**, 110893.

39 Y. Zhang, S. Xu, J. Liu, *et al.*, Carbon quantum dots enhanced polyurethane-urea nanocomposites with mechanical reinforcement and room-temperature self-healing performance, *Appl. Surf. Sci.*, 2024, **655**, 159645.

40 Y. Hou, H. Wu, Q. Wu, *et al.*, Recyclable elastomers with high mechanical performance and vibration-damping property via triple dynamic bonds, *Polymer*, 2024, **304**, 127161.

41 J. Wu, X. Wang, Y. Deng, *et al.*, Waterborne polyurethane acrylate emulsion with dangling chain structure: Simultaneously showing wide damping temperature range and excellent hydrophobic performance, *Polym. Adv. Technol.*, 2023, **34**(4), 1265–1278.

42 X. Han, D. Wang, X. Chen, *et al.*, High damping polyurethane elastomers with wide temperature ranges, *Polymer*, 2025, **325**, 128307.

43 J. Liu, S. Wang, *et al.*, Mechanical Robust, Self-Healable Polyurethane Elastomer Enabled by Hierarchical Hydrogen Bonds and Disulfide Bonds, *Polymers*, 2023, **15**(19), 4020.

44 S. Nevejans, N. Ballard, M. Fernández, *et al.*, The challenges of obtaining mechanical strength in self-healing polymers containing dynamic covalent bonds, *Polymer*, 2019, **179**, 121670.

45 M. Tian, S. Chattopadhyay, *et al.*, A tutorial review of linear rheology for polymer chemists: basics and best practices for covalent adaptable networks, *Polym. Chem.*, 2024, **15**(9), 815–846.

46 X. Wang, L. Wang, C. Liu, *et al.*, Self-Healing Polyurethane Elastomers with Superior Tensile Strength and Elastic Recovery Based on Dynamic Oxime-Carbamate and Hydrogen Bond Interactions, *Macromol. Rapid Commun.*, 2024, **45**(13), e2400022.

47 X. Zhu, K. Han, C. Li, *et al.*, Tough, Photoluminescent, Self-Healing Waterborne Polyurethane Elastomers Resulting from Synergistic Action of Multiple Dynamic Bonds, *ACS Appl. Mater. Interfaces*, 2023, **15**(15), 19414–19426.